International Journal of Rotating Machinery
1997, Vol. 3, No. 2, pp. 93–105
Reprints available directly from the publisher
Photocopying permitted by license only

Flow Measurements and Flow Analysis in the Exit Region of a Radial Turbine

D. M. MURUGAN[†], W. TABAKOFF* and A. HAMED

Department of Aerospace Engineering and Engineering Mechanics, University of Cincinnati, Cincinnati, Ohio, U.S.A

(Received April 1996; In final form 2 May 1996)

Three-dimensional flow measurements using LDV system were obtained in the exit region of a radial inflow turbine at an off-design operating condition. The measurements reveal a complex flow pattern near the tip region at the rotor exit due to the interaction of the tip clearance flow. The effect of the rotor on the exit flow field is observed in the proximity of the rotor exit. Steady axisymmetric, compressible, turbulent flow computations with a two equation turbulence model were performed using the PARC code for the meridional flow in the radial turbine exit region. The computational results obtained in the meridional plane are compared with the experimental results, which are correlated to the rotor blade rotation in the exit region of the radial turbine.

A version of this paper was presented at the 30th AIAA/ASME/SAE/ASEE Joint Propulsion Conference, Indianapolis, Indiana, Paper no. AIAA-94-3075.

Keywords: Turbomachinery, Turbomachinery Flows, Radial Turbomachinery, Radial Turbines, Radial Turbine Exit Flows, Radial Turbine Exit Flow Measurements and Flow Analysis.

INTRODUCTION

The increasing applications of the radial turbines necessitate better understanding of the flow behavior in order to optimize the design and minimize the losses. As part of an on-going research program on radial inflow turbine at the University of Cincinnati, Malak et al. [1986] measured the detailed flow field in the scroll cross-sections of a radial turbine using LDV system. Eroglu and Tabakoff [1989] investigated the flow field in the nozzle guide vane and Lakshminarasimha et al. [1989] reported the flow measurements in the vaneless free vortex region. All these investigations were performed without the rotor, which was replaced by an aluminum body of revolution. Recently Pasin and Tabakoff [1992] investigated

*Corresponding author.

[†]Currently Project Engineer, EASi Engineering, 30800 Telegraph Road, Suite 3700, Bingham Farms, MI 48025., Graduate Research Assistant.

the flow field inside the inlet guide vanes of the radial inflow turbine with the rotor. They observed the periodicity of the flow field in the inlet guide vane passages with the rotor revolution. Later, Pasin and Tabakoff [1993] performed flow measurements inside the rotor of the radial turbine.

The radial turbine exit flow field has been studied by some investigators such as Kofskey et al. [1972], Mclallin et al. [1980] and Szewczuk [1989]. Researchers like Rohlik et al. [1970] and Japikse et al. [1979] have reported in detail the performance of radial turbine exhaust diffusers. Zangeneh et al. [1988] compared the flow measurements and three-dimensional viscous computations of the flow field in a low speed radial inflow turbine including the turbine exit region. Kitson [1992] performed a detailed assessment of the various computational methods for the aerodynamic investigation of radial turbines.

In the present investigation, detailed flow measurements were obtained in the region downstream of a radial inflow turbine rotor at off-design condition using a three component Laser Doppler Velocimeter system and the measured flow velocities are correlated to various rotor blade positions. The results are examined to reveal the influence of swirl and turbulence on the radial inflow turbine exit flow field and associated losses. A limited numerical simulation was performed using the axisymmetric, compressible, turbulent viscous code, PARC with k-ε turbulence model in the meridional plane of the turbine exit region.

MAIN TEXT

Test Rig and Instrumentation

Referring to Fig. 1, the experimental set-up consists of the test turbine, the 3-dimensional LDV & Data acquisition systems and the air supply systems.

Radial Turbine and Laser Window

The test turbine is shown schematically in Fig. 2. The scroll has a nearly square cross-section, followed by 18 slightly cambered inlet guide vanes. Details on the scroll and the guide vanes can be found in the references by Malak et al. [1986] and Pasin et al. [1992]. The rotor has an inlet radius of 81.8 mm (3.22″). The exit hub and tip radii are 22.1 mm (0.87″) and 43.2 mm (1.7″) respectively. The rotor has 8 full blades and 8 splitter blades. The rotor blade span at the inlet and at the exit are 12.7 mm (0.50″) and 21.1 mm (0.83″) respectively. The rotor does not incorporate an exducer and so the rotor blades are axially straight at the exit. The exit duct wall has an inner radius of 44.5 mm (1.75″). The rotor hub at the exit of the rotor is smoothly shaped to guide the flow into the exit duct.

In order to have access for the laser beams, a measurement window made out of 1.3 mm (0.05″) thick Lexan material, was fixed on the turbine exit duct so that it follows the curvature of the duct wall. Detailed descriptions on the selection of this window material can be found in the reference by Murugan et al. [1994].

LDV System

The measurements were accomplished with a three component LDV system as shown in Fig. 1. The optics for the three component LDV were arranged in off-axis backward scatter mode. Blue and Green components were used to measure the horizontal and vertical velocity components respectively, while the purple component was used to measure the non-orthogonal velocity component that is inclined at 30° to the blue component in the same plane. The focal length of the transmitting lenses was 480 mm. Beam expanders were used to reduce the measuring volume diameter 3.75 times and to improve the signal-to-noise ratio. Frequency shifters were used to identify the flow direction and to reduce the fringe bias. The entire LDV system with the bread-board was mounted on a milling machine table, which can traverse 254 mm, 457.2 mm and 558.8 mm in the axial (longitudinal), transverse and vertical directions respectively with an accuracy of 0.025 mm (0.001″) in all the three directions. The characteristics of the LDV system used are summarized in Table I. A commercial six-jet atomizer, TSI 9306 model was used to

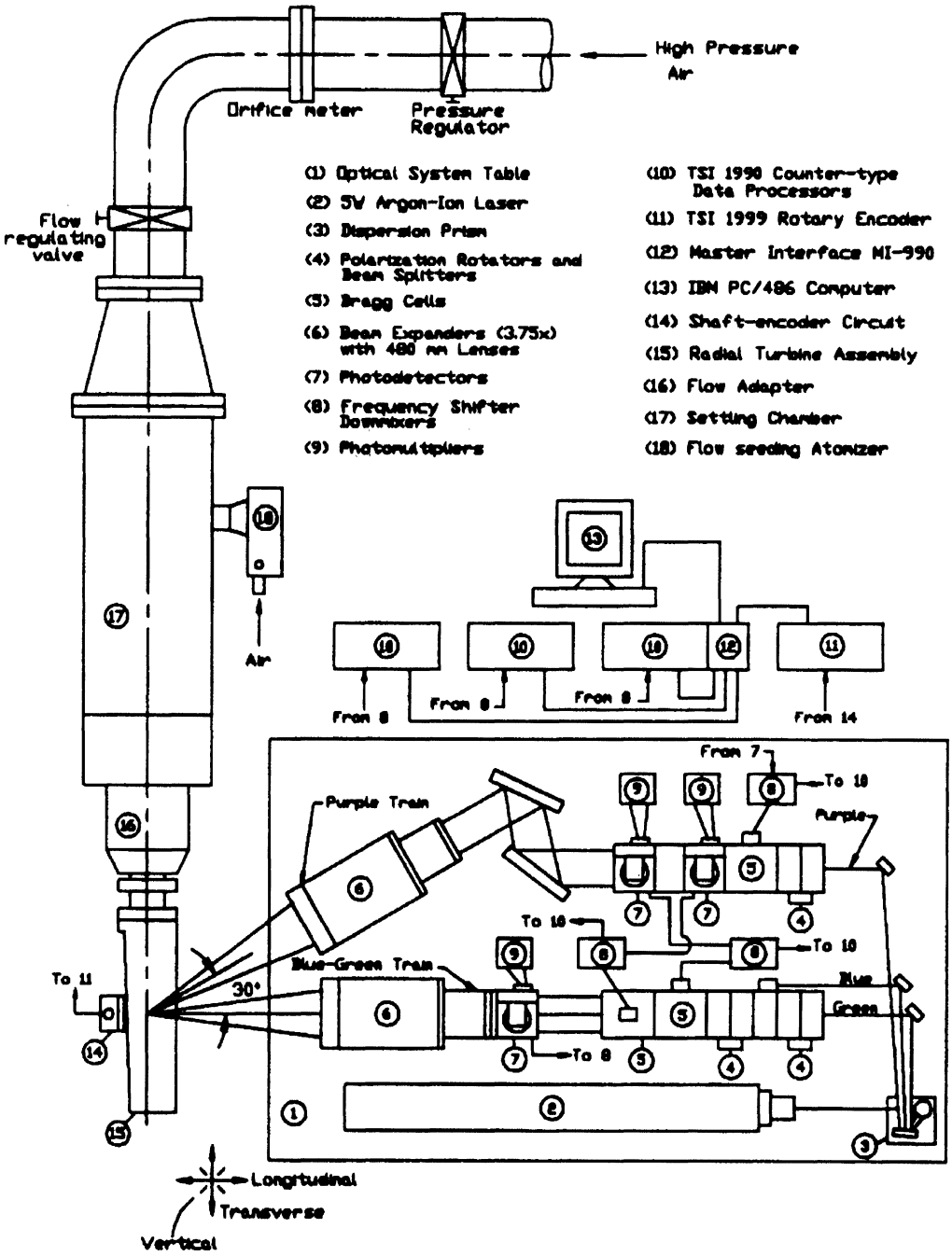

FIGURE 1 The LDV system and the test rig.

seed the flow with propylene glycol particles of 2 μm mean diameter. The atomizer is capable of generating particle concentrations of 10^5 particles/cm^3. The atomizer was connected to the bottom of the settling chamber through which the air enters into the turbine as shown in Fig. 1.

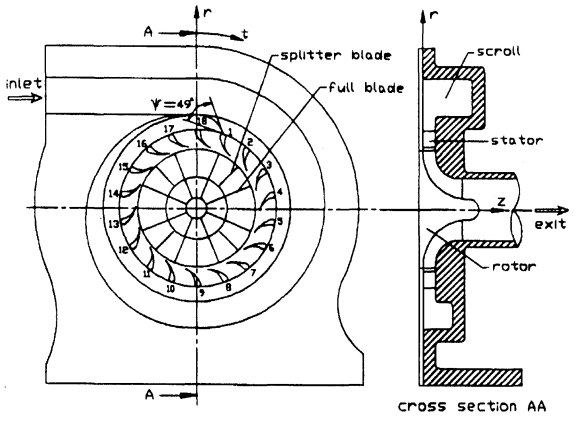

FIGURE 2 Sketch of the test turbine configuration.

Data Acquisition System

Three counter type signal processors (TSI Model 1990) and a rotary encoder (model TSI 1999) were used in the data acquisition. The signal processors send the processed data to a TSI MI-990 multi-channel interface, which is housed in one of the processors. Also, the MI-990 receives the rotor blade position information from the rotary encoder at the time of each velocity data measurement. The combined data are then sent from the MI-990 to an IBM P/C through an IBM 6260 DMA card.

Measurement Technique

In the test facility, it was possible to rotate the turbine rig about its inlet duct axis to a convenient angle in order to gain access into the exit region of the rotor as well as to synchronize the rotary shaft-angle encoder. From the directly measured velocity components, the orthogonal on-axis component was calculated through the following transformation relation:

$$W = \frac{V_b \cos\theta - V_p}{\sin\theta} \tag{1}$$

where V_b and V_p are the horizontal (blue) and non-orthogonal (purple) components of velocity respectively and θ is the inclination angle between the two optical trains. Due to the access constraints into the test rig, the angle, θ was set to 30°. The measured horizontal, vertical and axial (on-axis) components of the velocity were then transformed vectorially by the angle of inclination of the test rig to get the tangential, radial and axial components of the velocity in the exit duct. The mean ensemble averaged value of each component velocity is defined as:

$$\overline{U}_{i,j} = \frac{\sum_{k=1}^{N_{i,j}} U_{i,j,k}}{N_{i,j}} \tag{2}$$

where $N_{i,j}$ is the number of velocity data at the measurement location 'i' for the rotor position 'j'. In a similar way, the variance of the corresponding velocity component for the same rotor position 'j' at the measurement location 'i' is defined as follows:

$$\sigma_{i,j}^2 = \frac{\sum_{k=1}^{N_{i,j}} (U_{i,j,k} - \overline{U}_{i,j})^2}{N_{i,j} - 1} \tag{3}$$

where $\sigma_{i,j}$ is the standard deviation or the turbulence level of the corresponding velocity component.

Measurement Errors

Like other measurement techniques, the LDV measurement introduces some fixed bias errors, called systematic uncertainties as well as some random errors, called statistical uncertainties. The statistical uncertainties in the measured mean velocities were estimated using the procedures described by Snyder et al. [1981, 1984]. The uncertainty interval of a measured quantity can be related to the sample size as follows (Snyder et al. [1984]):

$$\Delta U = \pm \frac{z S_u}{\sqrt{N}} \tag{4}$$

where S_u is an estimate for the true standard deviation and N is the sample size. The value of z is 1.96 for 95% confidence level. Based on this statistical analysis, the data sample size for each angular position of the rotor blade was determined to be 400.

TABLE I LDV characteristics

Characteristics	Blue	Green	Purple
Wavelength in μm	0.488	0.5145	0.4765
Fringe Spacing in μm	2.851	3.0	2.784
Diameter of measuring volume at e^{-2} intensity location in mm	0.053	0.056	0.052
Length of measuring volume at e^{-2} intensity location in mm	0.617	0.651	0.603
Number of stationary fringes	19	19	19

With this sample size, the statistical uncertainty in the total velocity was found to be ±2.5% and the uncertainty in the flow angle (α_{rz}) was found to be ±3° close to the rotor exit near blade mid span. The systematic uncertainties were also calculated as described by Snyder et al. [1981]. A summary of the relative uncertainties associated with the measurements are given in Table II.

TABLE II Systematic measurement uncertainties

Longitudinal, transverse & vertical traverses	±0.025 mm (0.001″)
Optical axis or turbine rig angular orientation	±0.5°
Horizontal Velocity Component ($\Delta U_b/U_{bm}$)	±1.63%
Vertical Velocity Component ($\Delta U_g/U_{gm}$)	±1.63%
On-axis Velocity Component ($\Delta W/W_m$)	±12.92% (ϕ = 0°) ±11.87% (ϕ = 45°) ±3.86% (ϕ = 90°)

Numerical Analysis

A limited numerical simulation of the flow field in the meridional plane of the radial turbine exit region has been performed neglecting the tip-clearance flow and the rotor rotational effect. The flow field simulations are based on the implicit solution of the compressible Navier-Stokes equations in the strong conservation form and general curvilinear coordinates. The steady, axisymmetric, compressible, turbulent viscous code, "PARC" [1989] with the two-equation k-ε turbulence model was used in the computation of the flow field. This code uses the Beam and Warming scheme modified with the diagonalized algorithm for the solution of the governing equations. The PARC code has been extensively used with good success to solve propulsion inlet and exhaust nozzle problems. Fig. 3 shows the grid structure for the flow field in the tested radial turbine exit region configuration. Referring to Fig. 3, a total of 7701 grid points were used in the flow field discretization with a 151 × 51 mesh. A two-dimensional poisson grid generation scheme with grid stretching was used to maintain the y^+ value of the near wall grid point less than 2.0, thus ensuring at least 20 grid points in the boundary layer along all solid wall boundaries. The measured total pressure and temperature were given as the initial conditions at inlet to the exit duct. During the simulation, the exit static pressure was controlled to obtain the same mass flow as that of the experiment. The rest of the

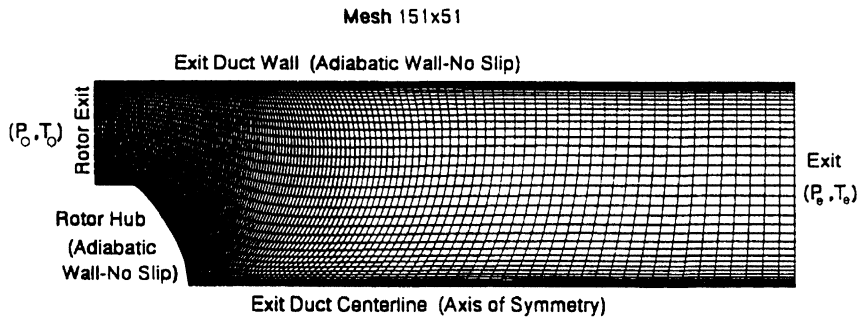

FIGURE 3 Computational mesh of the exit duct and boundary conditions

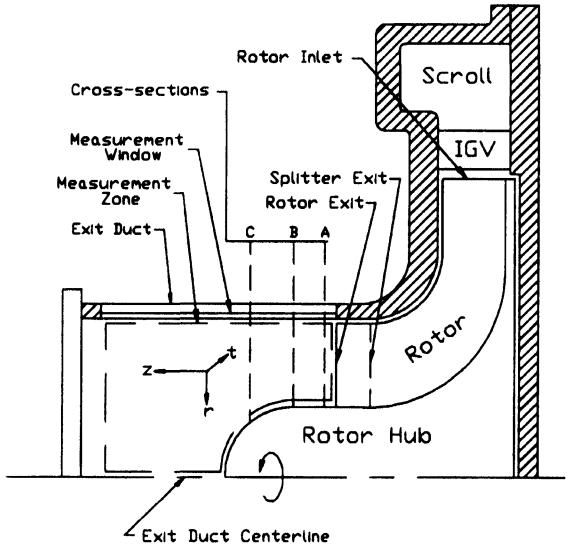

FIGURE 4 Sketch showing the radial turbine exit and the measurement zone.

boundary conditions used in the simulation of the flow field are given in Fig. 3. The computations required approximately 20,000 iterations at 0.4 CFL number to converge to steady state solution. The criteria for convergence were that the order of magnitude reductions in the averaged root mean square error of the flux be 9 times and the order of magnitude reductions in the percentage local maximum error of the density be 4 times.

Results and Discussion

Experimental Results

Referring to Fig. 4, the LDV measurements downstream of the radial turbine rotor were obtained in the cross-sectional planes (A, B and C) and also in the meridional plane. Fig. 4a shows three-dimensional sketch of the turbine exit region with the measurement cross-sectional planes. All the experimental results reported in this paper were obtained at a constant mass flow rate of 0.055 kg/s (0.121 lb/s) and a constant turbine speed of 1000 rpm. The Reynolds number and the Mach number were 0.564×10^5 and 0.04 respectively based on cold air properties at

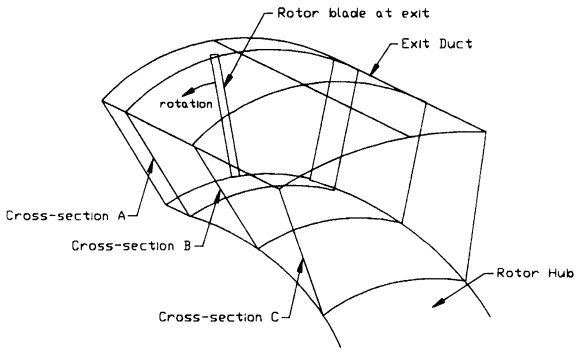

FIGURE 4A Three-dimensional sketch of the measurement cross-sections.

21.1°C (70°F), the mean diameter at the rotor exit, and the time and passage averaged absolute velocity at the rotor exit (which was 12.2 m/s for the tested conditions). The results are presented as vector and contour plots of the measured parameters in the cross-sectional planes A, B and C as well as in the meridional plane. The notations of the measured mean flow velocity directions and flow angles are shown in Fig. 5. The mean velocity components presented in the plots are the absolute velocity components in the tangential, radial and axial directions from mid-passage to mid-passage, covering one rotor blade passage.

The results obtained in the first cross-section A, which is located at 2.54 mm (0.1″) downstream of the rotor exit are explained in this paragraph. According to the tangential velocity contour plot, shown in Fig. 6(a), the tangential velocities of the fluid exiting along the pressure surface are higher compared to those along the suction surface. Near the tip region, gross under turning of the flow is observed at the exit of this exducerless radial turbine and hence the degree of swirl is very high near the tip region. This

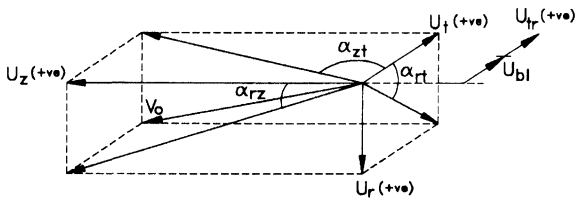

FIGURE 5 Flow velocity vectors and flow angle notations.

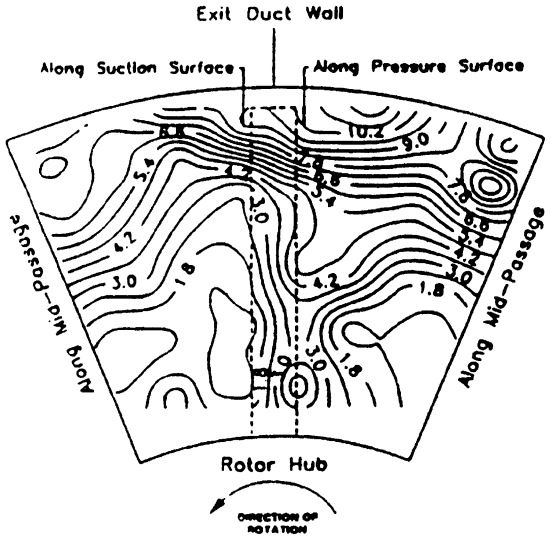

FIGURE 6(A) Tangential velocity contours (U_t – m/s) [cross-section A].

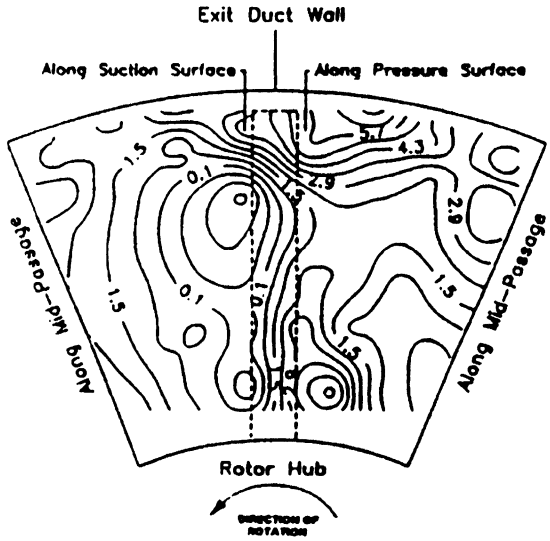

FIGURE 6(B) Radial velocity contours (U_r – m/s) [cross-section A].

observation is in good agreement with the results of Kitson [1992]. The work extracted from the fluid as determined from the velocity triangles at the rotor inlet and exit leads to the fact that the high degree of swirl near the tip region drastically reduces the work loading in that region and is hence detrimental to the overall performance. The radial velocity contours, presented in Fig. 6(b), show that there is a general radially inward movement (towards the rotor hub) of the flow due to the loss of the centrifugal force as the flow leaves the rotor. This phenomenon is also reported by Kitson [1992]. The radial velocities are generally low throughout the cross-section except near the pressure surface tip corner region, which may be due to the possible increased interaction of the tip clearance flow with the main flow. It is possible that the mixing of the tip clearance flow with the main flow is enhanced near the pressure surface since the streamwise momentum of the flow near the pressure surface is low, which is also evidently seen in the mean velocity vector plot in the meridional plane along pressure surface in Fig. 9(a). The axial velocity contours are shown in Fig. 6(c) and they are higher along the suction surface than those along the pressure surface.

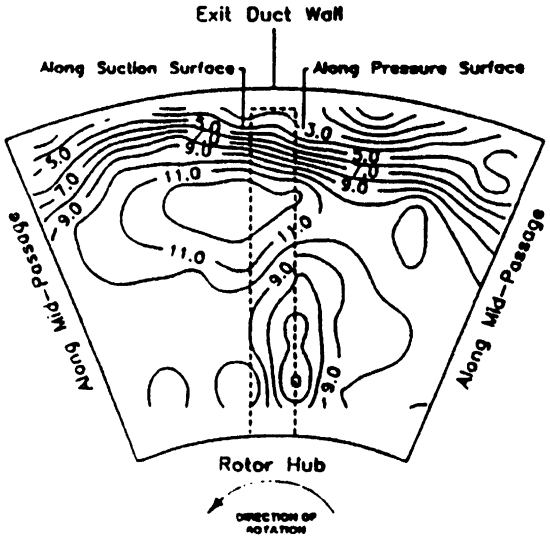

FIGURE 6(C) Axial velocity contours (U_z – m/s) [cross-section A].

The next set of results, Fig. 7(a) through Fig. 7(c), were obtained at the cross-section B, which is located at 7.62 mm (0.3″) downstream of the rotor exit. The tangential velocity contours, shown in Fig. 7(a) exhibit no significant variation from the pressure side to the suction side. This indicates that the flow behind

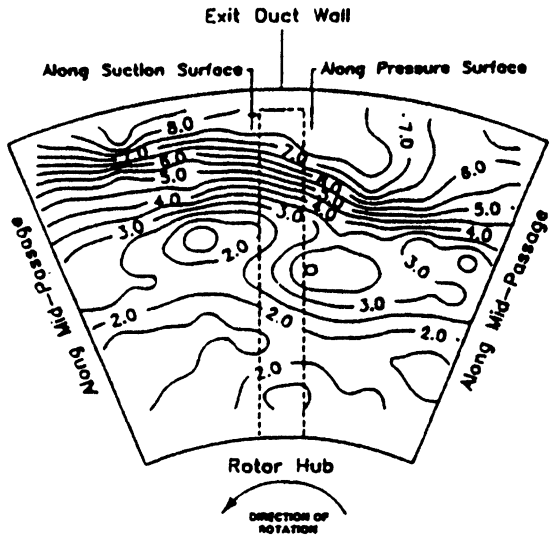

FIGURE 7(A) Tangential velocity contours (U_t – m/s) [cross-section B].

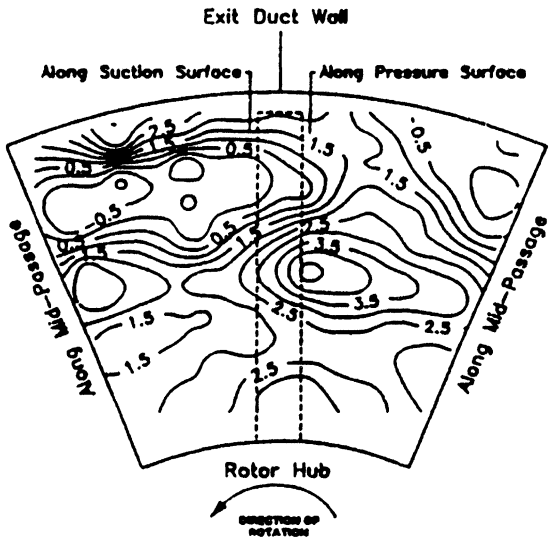

FIGURE 7(B) Radial velocity contours (U_r – m/s) [cross-section B].

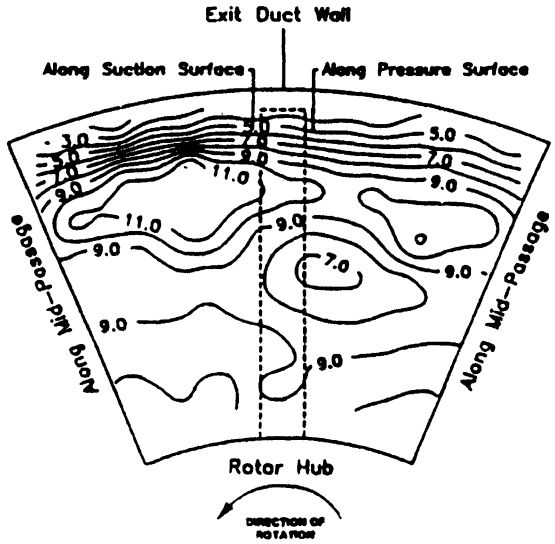

FIGURE 7(C) Axial velocity contours (U_z – m/s) [Cross-Section B].

the trailing edge of the rotor blade is completely mixed at this station. In addition, the tangential velocities are reduced compared to their values at cross-section A. The radial velocity contours, shown in Fig. 7(b) are generally low in the upper half but higher in the lower half of the cross-section, where the flow starts to turn radially inward near the hub-end (see also Fig. 4). The axial velocity contours, shown in Fig. 7(c), indicate they are mostly uniform except in small zones near the tip along the suction surface.

The results of the cross-section C, which is located at 15.24 mm (0.6″) downstream of the rotor exit are explained in this paragraph. The tangential velocities for this cross-sectional plane are shown in Fig. 8(a). They are almost uniform along the tangential direction at each radial location and the levels of the tangential velocities are less than those of the cross-section B. Comparing the tangential velocity contour plots of the three cross-sections, it can be noted that the degree of swirl decreases in the downstream direction. The radial velocity contours, shown in Fig. 8(b), are generally low throughout the cross-section. The radial velocities near the hub along mid-passage are slightly negative due to the wake behind the hub-end. The wake generated behind the hub-end blocks the flow near the duct centerline and deflects the main flow slightly in the radially outward direction. The axial velocity contours as shown in Fig. 8(c) indicate slightly higher values just above the hub.

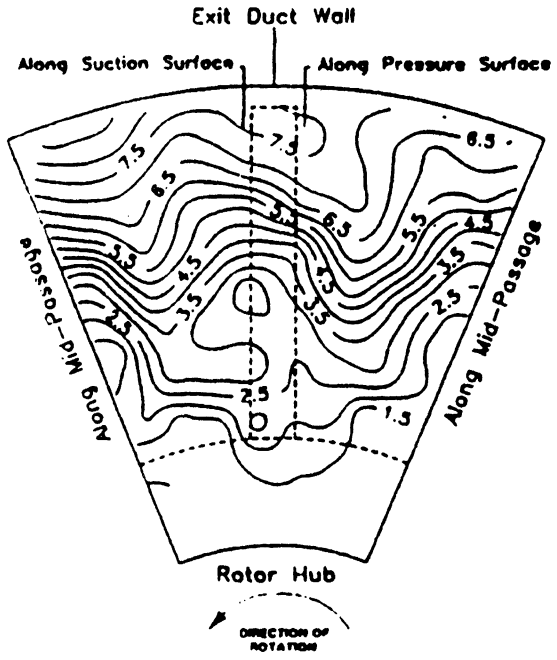

FIGURE 8(A) Tangential velocity contours (U_t – m/s) [cross-section C].

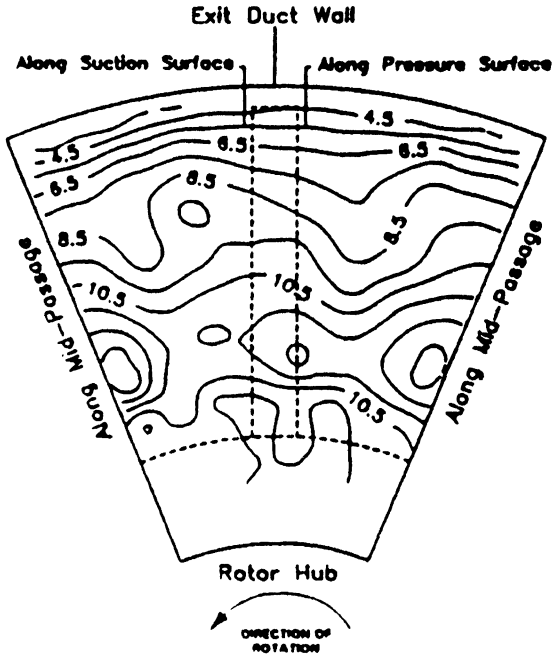

FIGURE 8(C) Axial velocity contours (U_z – m/s) [cross-section C].

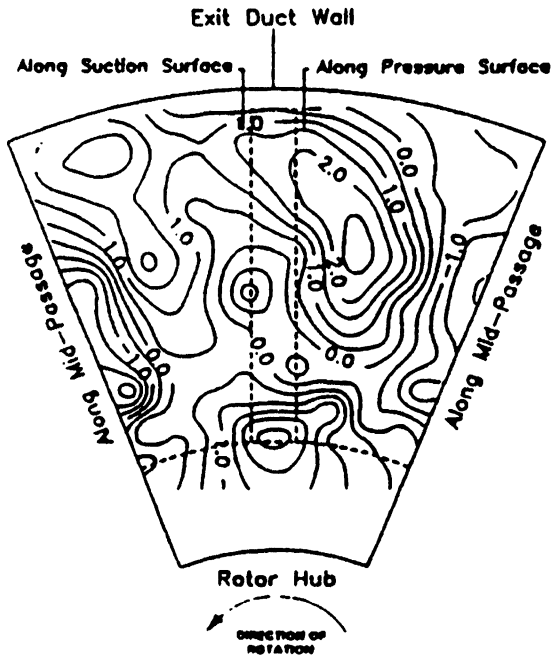

FIGURE 8(B) Radial velocity contours (U_r – m/s) [cross-section C].

The measured meridional flow velocity vectors for three different rotor blade positions are presented in Figures 9(a) through 9(c). Fig. 9(a) shows the meridional velocity vector plot in a plane aligned with the blade pressure surface. Due to the low meridional velocities near the pressure surface, it is possible for the tip clearance flow to penetrate deep in the radial direction and mix with main flow near the tip region. The meridional velocity vector plot in a plane aligned with the rotor mid-passage is shown in Fig. 9(b). The meridional velocity vectors in a plane aligned with the blade suction surface are shown in Fig. 9(c). Comparing Figures 9(b) and 9(c) with Fig. 9(a), one can observe the reduced influence of the tip clearance flow at the times of passing of the rotor mid-passage and the blade suction surface.

From the three Figures 9(a) through 9(c), we can conclude that the flow field near the rotor exit is highly complex due to the interaction of the tip clearance flow, the wake region behind the hub-end and the boundary layer development on the duct wall. The exit flow velocities increase in the mid-region

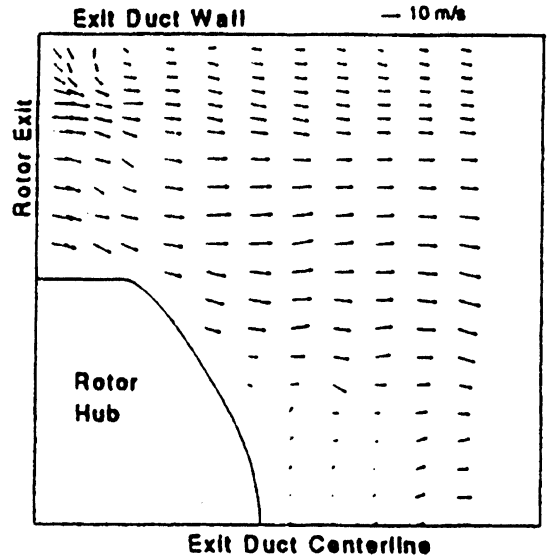

FIGURE 9(A) Vector plot of mean velocity in the meridional plane [along pressure surface].

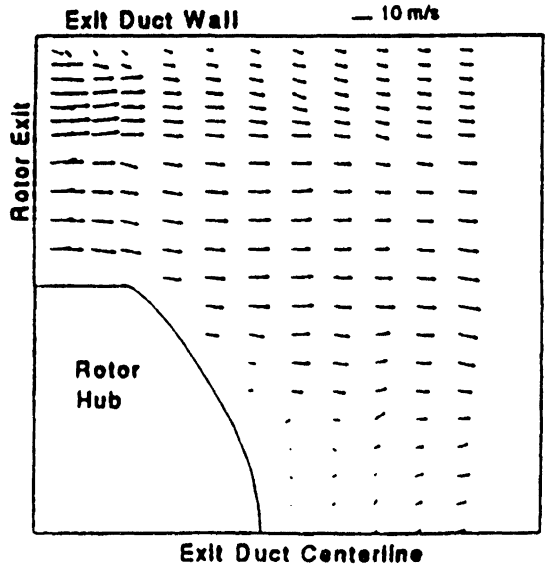

FIGURE 9(C) Vector plot of mean velocity in the meridional plane [along suction surface].

due to the blockage caused by the wake region behind the hub-end and the boundary layer on the duct wall. Figures 9(a) through 9(c) indicate that the rotor

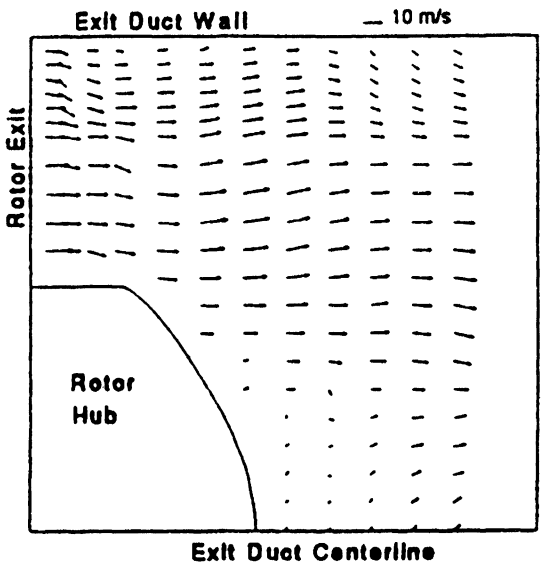

FIGURE 9(B) Vector plot of mean velocity in the meridional plane [along mid-passage].

blade influence diminishes further downstream of the straight portion of the hub, after which the flow field is similar for all rotor blade positions.

Computational Results and Comparison

The computed axisymmetric flow field vector plot, obtained from the PARC code in the turbine exit region near the rotor exit, is shown in Fig. 10. In this figure, the separation behind the rotor hub is clearly captured. However, the effects of the tip clearance flow and the rotor rotation were not simulated in the predictions.

The computational results are compared with the experimental measurements obtained in the meridional plane along mid-passage, since it exhibits the least influence of the rotor blade. In the figures 11(a) and 11(b), it can be seen that with regard to the point of separation on the hub end, the agreement between the experiment and the numerical results is poor. This can be due to the fact that the rotation of the rotor hub is neglected in the analysis. The rotation of the rotor hub can cause more turbulence in the flow field around it and this increased turbulence could be the

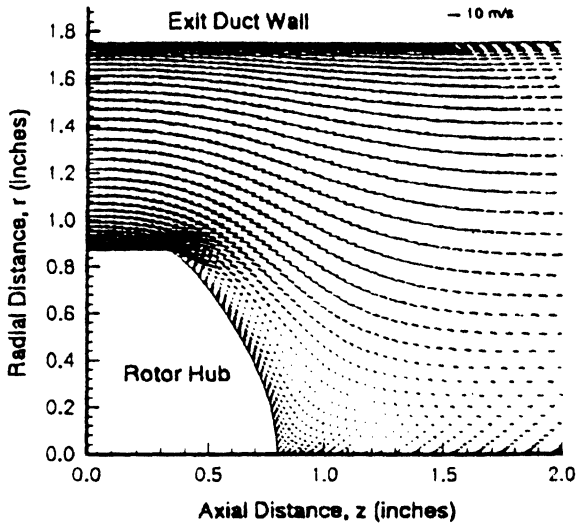

FIGURE 10 Vector plot of the flow field in the meridional plane [computational].

reason for the delayed separation on the hub-end as obtained in the experiment. On the other hand, the predicted and experimental reattachment points of separation behind the hub end are nearly at the same location, approximately 1.2″ from the rotor blade exit. Hence, the prediction of the reattachment point of this separation agrees very well with that of the experiment. Good agreement between the experiment and the prediction also exists, as far as the acceleration of the flow in the mid region just above the end of the straight portion of the rotor hub.

PRACTICAL IMPORTANCE

An unresolved problem that is still encountered by the designers is the relatively high loss region near the shroud at the exit plane of the radial turbine rotor. This high loss region, which also corresponds to the region of high swirl, is further worsened under off-design conditions. The swirl and the turbulence in the exit flow field can significantly contribute to the generation of noise and vibration of the unit. This investigation identifies the radial turbine exit loss producing mechanisms, namely the high-swirl flow near the rotor tip, the mixing patterns of the tip clearance flow and the wake behind the rotor hub. The results of this and the preceding (Pasin and Tabakoff [1993]) experimental investigations inside and downstream of the radial turbine rotor conducted at an off-design condition provide a database for validating three-dimensional turbomachinery CFD codes. The limited computational investigation of this work helps us to un-

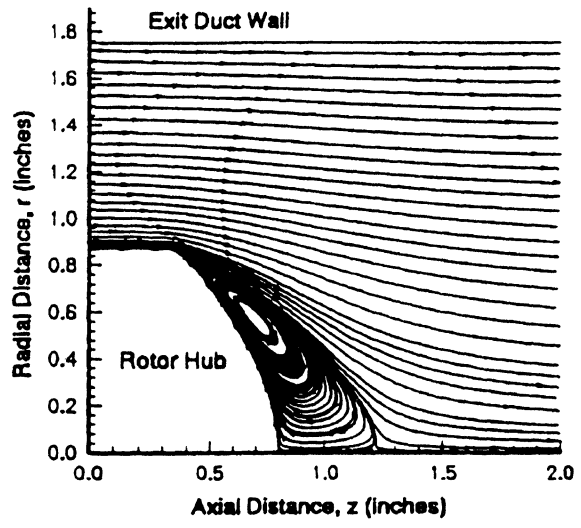

FIGURE 11(A) Streamline plot of the flow field in the meridional plane [computational].

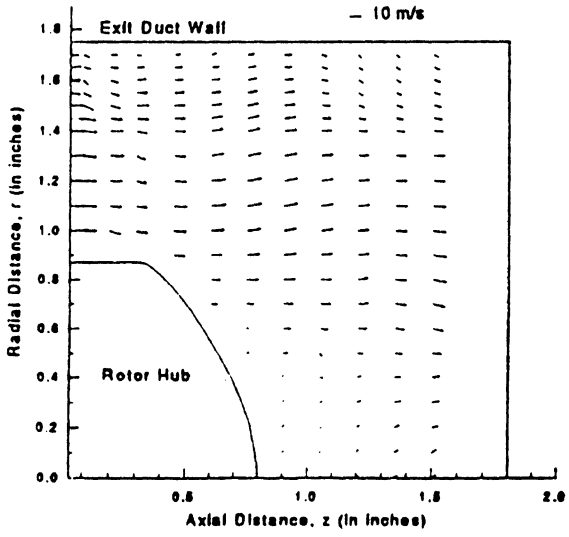

FIGURE 11(B) Vector plot of the flow field in the meridional plane [experimental] [Along Mid-Passage].

derstand the effect of the wake behind the rotor hub and its interaction with the turbine exit flow field. However, more detailed, three-dimensional computational studies should be undertaken in order to achieve good prediction of the highly complex flow field inside and at the exit of a radial turbine.

CONCLUSIONS

An experimental investigation and limited analysis of the exit flow field of a radial turbine were conducted at off-design condition. The flow field in the immediate vicinity of the rotor tip is influenced by the tip clearance flow. The mixing of the tip clearance flow with the main flow is revealed at different locations relative to the rotor blade position. The degree of swirl of the flow near the tip region at the rotor exit is very high due to the gross under turning of the flow near this region. The swirl of the flow near the pressure surface was found to be higher than that near the suction surface at the measurement cross-sectional plane nearest to the rotor exit. The degree of swirl reduces as the flow mixes and is guided downstream in the exit duct. The wake behind the hub and the boundary layer development on the exit duct wall are captured in this investigation.

A limited simulation of the flow field in the meridional plane of the radial turbine exit flow field has been performed. This limited simulation gives a good understanding of the nature of the wake behind the rotor hub and its interaction with the turbine exit flow field.

Acknowledgment

This research was supported by NSF Contract No. CTS-9012309 during 1990–1993. The authors also express their thanks to the Ohio Super Computer Center for granting permission to use the OSC super computer resources for the flow computations.

NOMENCLATURE

IGV	Inlet Guide Vane
LDV	Laser Doppler Velocimeter
N	data sample size
P	pressure
r	radial direction
t	tangential direction
T	temperature
U, V	velocity components
	mean value of velocity component
U_{bl}	rotor blade velocity
W	on-axis velocity component
z	axial direction
$\Delta U, \Delta V$	measurement uncertainty of velocity component U, V
α	absolute flow angle
σ	standard deviation in a velocity data sample
θ	LDV coupling angle between the purple optical axis and the blue-green optical axis
ϕ	angle between the in-plane resultant velocity and the blue component velocity

SUBSCRIPTS

b	blue component
e	exit
g	green component
i	measurement point
j	rotor blade position
m	mean value
o	total condition
p	purple component
r	radial component
rz	radial-axial plane
rt	radial-tangential plane
t	tangential component
z	axial component
zt	axial-tangential plane

References

Cooper, G.K. and Sirbaugh, J.R. (1989). PARC Code: Theory and Usage, *AEDC-TR-89-15*, December, Arnold Engineering Development Center, Tennessee.

Hassan Eroglu and Widen Tabakoff (1989). LDV Measurements and Investigation of Flow Field Through Radial Turbine Guide Vanes, *ASME paper no.* 89-GT-162.

Japikse, D. and Pampreen, R. (1979). Annular Diffuser Performance for an Automotive Gas Turbine, *Trans. ASME Journal of Engineering for Gas Turbine and Power*, Vol. 106, pp. 358–372.

Kitson, S.T. (1992). Aerodynamic Investigation of Radial Turbines Using Computational Methods, *VKI Lecture Series* 1992-05, April 6–10, pp. 1–44.

Kofskey, M.G. and Nusbaum, W.J., (1972). Effects of Specific Speed on Experimental Performance of a Radial Inflow Turbine, *NASA TN-D-6605.*

Lakshminarasimha, A.N., Tabakoff, W. and Metwally, A.M. (1989). LDV Measurements and the Flow Analysis in the Vaneless Region of a Radial Inflow Turbine, *ASME paper no.* 89-GT-122.

Malak, M.F., Hamed, A. and Tabakoff, W. (1986). Three Dimensional Flow Field Measurements in a Radial Inflow Turbine Scroll using LDV, *ASME paper no.* 86-GT-122.

Mclallin, K.L. and Haas, J.E. (1980). Experimental Performance and Analysis of 15.04 cm Tip Diameter Radial-Inflow Turbine with Work Factor 1.126 and Thick Blading, *NASA Tech. paper no.* 1730.

Murugan, D.M., Tabakoff, W. and Hamed, A. (1994). Flow Field Investigation in the Exit Region of a Radial Inflow Turbine Using LDV, *ASME paper no.* 94-GT-101.

Pasin, M. and Tabakoff, W. (1992). Laser Measurements of Unsteady Flow Field in a Radial Turbine Guide Vanes, *30th Aerospace Sciences Meeting & Exhibit*, Jan., paper no. AIAA 92-0394.

Pasin, M. and Tabakoff, W. (1993). Laser Measurements of the Flow Field in a Radial Turbine Rotor, *31st Aerospace Sciences Meeting & Exhibit*, Jan., paper no. AIAA 93-0156.

Rohlik, H.E., Kofskey, M.G. and Nusbaum, W.J. (1970). Radial Inflow Turbine Performance with an Exit Diffuser Designed for Linear Static Pressure Variation, *NASA-TM-X-52890.*

Snyder, P.K., Orloff, K.L. and Aoyagi, K. (1981). Performance and Analysis of a Three Dimensional Non-Orthogonal Laser Doppler Anemometer, *NASA TM-81283.*

Snyder, P.K., Orloff, K.L. and Reinath, M.S. (1984). Reduction of Flow Measurement Uncertainties in Laser Velocimeters with Nonorthogonal Channels, *AIAA Journal*, August, Vol. 22, No. 8, pp. 1115–1123.

Szewczuk, S. (1989). A Review of their Characteristics and an Experimental Investigation and Analytical Prediction of the Aerodynamic Performance of a 9.6 cm Radial Inflow Turbine, *ISABE proceedings* ISABE 89-7042, pp. 419–426.

Zangeneh-Kazemi, M., Dawes, W.N. and Hawthorne, W.R. (1988). Three Dimensional Flow in Radial-Inflow Turbines, *ASME paper no.* 88-GT-103.

MANEY
publishing

The Institute of Materials, Minerals & Mining

ENERGY MATERIALS

NEW FOR 2006

Materials Science & Engineering for Energy Systems

Maney Publishing on behalf of the Institute of Materials, Minerals and Mining

Economic and environmental factors are creating ever greater pressures for the efficient generation, transmission and use of energy. Materials developments are crucial to progress in all these areas: to innovation in design; to extending lifetime and maintenance intervals; and to successful operation in more demanding environments. Drawing together the broad community with interests in these areas, *Energy Materials* addresses materials needs in future energy generation, transmission, utilisation, conservation and storage. The journal covers thermal generation and gas turbines; renewable power (wind, wave, tidal, hydro, solar and geothermal); fuel cells (low and high temperature); materials issues relevant to biomass and biotechnology; nuclear power generation (fission and fusion); hydrogen generation and storage in the context of the 'hydrogen economy'; and the transmission and storage of the energy produced.

As well as publishing high-quality peer-reviewed research, *Energy Materials* promotes discussion of issues common to all sectors, through commissioned reviews and commentaries. The journal includes coverage of energy economics and policy, and broader social issues, since the political and legislative context influence research and investment decisions.

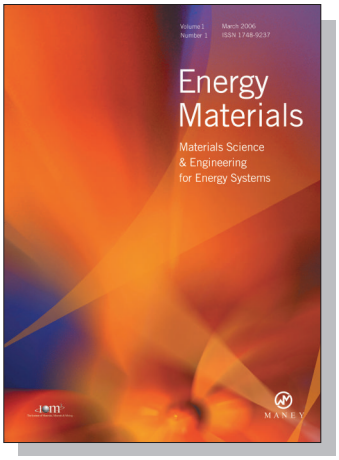

CALL FOR PAPERS

Contributions to the journal should be submitted online at **http://ema.edmgr.com**

To view the Notes for Contributors please visit: **www.maney.co.uk/journals/notes/ema**

Upon publication in 2006, this journal will be available via the Ingenta Connect journals service. To view free sample content online visit: **www.ingentaconnect.com/content/maney**

SUBSCRIPTION INFORMATION

Volume 1 (2006), 4 issues per year
Print ISSN: 1748-9237 Online ISSN: 1748-9245
Individual rate: £76.00/US$141.00
Institutional rate: £235.00/US$435.00
Online-only institutional rate: £199.00/US$367.00
For special IOM^3 member rates please email **subscriptions@maney.co.uk**

For further information please contact:
Maney Publishing UK
Tel: +44 (0)113 249 7481 Fax: +44 (0)113 248 6983 Email: subscriptions@maney.co.uk
or
Maney Publishing North America
Tel (toll free): 866 297 5154 Fax: 617 354 6875 Email: maney@maneyusa.com

For further information or to subscribe online please visit
www.maney.co.uk